Biomaterials Science

ROYAL SOCIETY OF CHEMISTRY

PAPER

View Article Online
View Journal | View Issue

Cite this: *Biomater. Sci.*, 2022, **10**, 947

Bioactive PCL microspheres with enhanced biocompatibility and collagen production for functional hyaluronic acid dermal fillers†

Yun Heo, ‡[a] Sang-Woo Shin,‡[a] Da-Seul Kim, [a,b] Semi Lee,[a] So-Yeon Park,[a,c] Seung-Woon Baek, [a,d,e] Jun-Kyu Lee, [a] Jun Hyuk Kim[a] and Dong Keun Han *[a]

Polymeric microspheres containing magnesium hydroxide (MH) and a bioactive agent (BA), such as apocynin (APO) and astaxanthin (ATX), have been prepared as functional dermal fillers with enhanced physicochemical and biological performance. In this study, polycaprolactone (PCL)-based microspheres were produced with a uniform size of about 30–40 μm by utilizing a membrane emulsification device. MH from the PCL/MH microspheres effectively neutralized acidic products from PCL degradation. For *in vitro* cell experiments, when acidic degradation products (6-hydroxycaproic acid, HCA) were treated with MH, the acidic pH was neutralized to induce wound healing and suppress inflammation. The microspheres comprised of BA had a sustained release of the BA, without an initial burst release. Remarkably, the ATX added into the microspheres was maintained for 16 weeks and displayed positive attributes, such as tissue regeneration and collagen production improvement, as noted by *in vivo* testing. Overall, these results suggest that the bioactive PCL microspheres containing ATX have excellent potential as a functional dermal filler for skin aesthetics and facial plastic surgery.

Received 2nd December 2021,
Accepted 4th January 2022

DOI: 10.1039/d1bm01846a

rsc.li/biomaterials-science

1. Introduction

As the aging population gradually increases, the demand and interest in skincare continue to grow. In particular, a procedure for removing wrinkles is drawing the most attention in the skin aesthetics field. Facial wrinkles are caused by fibrosis and collagen loss due to aging skin cells.[1] In general, there are three types of wrinkle removal procedures. First, botox is a muscle relaxant using botulinum toxin.[2] This has the advantage of a short treatment time and recovery period but has disadvantages such as being effective only for facial nerve palsy, limited treatment sites, and thin wrinkles.[3] Second, rhytidectomy, commonly known as face lifts, is a surgical procedure in which a polymer material, polydioxanone (PDO), is injected through a thread.[4] This is effective not only for wrinkles but also for improving skin sagging and facial lines. However, it is susceptible to infection, and may cause dimpling (a phenomenon in which the skin is temporarily depressed).[5] Lastly, dermal fillers are a treatment method that has been used for over 100 years for skincare purposes, where the end characteristics depend upon the material used.[6]

The first filler treatments (soft tissue augmentation) used paraffin and autologous fat. Paraffin was often used as it was deemed safe and was inexpensive, but problems existed, such as the formation of paraffinoma or displacement of implants.[7] Autologous fat transplantation takes a long time to perform and, once engrafted, fat is difficult to remove.[8] Fillers made of silicone began to attract attention during 1950–1960s. However, the silicone filler is not absorbed, and remains semi-permanent *in vivo*. As a result, the patient is exposed to the risk of skin necrosis due to foreign body reactions and inflammation.[9] In the 1980s, collagen extracted from animal skin was approved by the FDA as a filler.[10] However, collagen fillers have a short maintenance period and disadvantages such as allergic reactions and immune side effects.[11] Recently, hyaluronic acid (HA) has become the most widely used biomaterial for filler manufacturing.[12–14] HA is a linear polysaccharide that exists naturally in the skin, has high viscosity, and binds well

[a]*Department of Biomedical Science, CHA University, Seongnam-si, Gyeonggi 13488, Republic of Korea. E-mail: dkhan@cha.ac.kr*
[b]*School of Integrative Engineering, Chung-Ang University, Dongjak-gu, Seoul 06911, Republic of Korea*
[c]*Division of Biotechnology, College of Life Sciences and Biotechnology, Korea University, Seongbuk-gu, Seoul 02841, Republic of Korea*
[d]*Department of Biomedical Engineering, SKKU Institute for Convergence, Sungkyunkwan University (SKKU), Suwon-si, Gyeonggi 16419, Republic of Korea*
[e]*Department of Intelligent Precision Healthcare Convergence, SKKU Institute for Convergence, Sungkyunkwan University (SKKU), Suwon-si, Gyeonggi 16419, Republic of Korea*

†Electronic supplementary information (ESI) available. See DOI: 10.1039/d1bm01846a

‡These authors equally contributed to this work.

with water molecules through hydrogen bonds.[15] The HA-based filler was approved by the FDA in 2003. Since then, many pharmaceutical and biomedical companies have begun to design HA fillers.[16–18] HA is a substance that exists *in vivo*, has a low risk of allergy, and has excellent biocompatibility as it can be easily degraded by the endogenous enzyme, hyaluronidase, present in the body.[19,20] The HA is chemically cross-linked, and used as a dermal filler. In addition, the cross-linked HA is converted from a viscous liquid to a hydrogel, resulting in better physicochemical properties, and enhanced persistence as a filler.[21] However, the cross-linked HA fillers, like many other fillers, have a short duration of less than one year.[22]

Recently, several studies have been conducted to increase the duration of fillers using biodegradable polymers.[23–25] Polycaprolactone (PCL) is one such polymer and has a slow biodegradation rate due to its high crystallinity and hydrophobicity.[26] Ellanse™ (Sinclair Pharma, UK) is a filler made of 70% carboxymethyl cellulose gel and 30% PCL microspheres and has a duration time from nine months to four years.[27] FillerX™ (GANA R&D, Korea) was developed to extend the duration time from 2 to 4 years by adding PCL microspheres to the cross-linked HA-based filler.[28] Although PCL increased the duration time of the filler, hydroxycaproic acid (HCA), produced by the hydrolysis of PCL, acidifies the surrounding environment and causes an inflammatory reaction.[29] To overcome this limitation, magnesium hydroxide (MH) was used in this study. MH is a non-toxic and biocompatible ceramic, which is widely used as an antacid.[30] Research has shown that medical devices, such as scaffolds and stents that use a combination of biodegradable polymers and MH successfully inhibit the inflammatory response that occurs after implantation *in vivo*.[29,31] This is attributed to MH neutralizing acidic substances generated during the degradation of biodegradable polymers.

In this study, several bioactive agents (BA) were added to enhance the functionality of the filler. These antioxidants remove free radicals from cells, protect cells from oxidative stress, and inhibit cell aging. Apocynin (APO) is a natural compound found in *Apocynum cannabinum* and is a known inhibitor of NADPH oxidase.[32] It has been shown to prevent aging in dermal cells as well as in various other types of cells.[33] In addition, astaxanthin (ATX) is a substance in micro-algae and reddish seafood, such as shrimp and salmon, and promotes collagen production by reducing MMP1 in human dermal fibroblasts.[34] Given this information, we hypothesized that fillers containing microspheres with MH and BA could have the following advantages. MH could neutralize acidic degradation products, suppress inflammation, and slow the rate of hydrolysis of polymers, enhancing the stability of implanted fillers. The BA added to microspheres could inhibit free radicals, alter age-related gene expression, prevent aging of dermal tissues, and promote collagen production to maintain skin elasticity. Taken together, the addition of microspheres containing MH and BA could enhance physicochemical and biological performance as a dermal filler.

2. Materials and methods

2.1 Materials

Polycaprolactone (PCL; average M_w: 80 kDa) and polyvinyl alcohol (PVA; 87–90% hydrolyzed, average M_w: 30–70 kDa) were obtained from Sigma-Aldrich (St Louis, MO, USA). Magnesium hydroxide (MH; average particle size: 50 nm) and dichloromethane (DCM) were purchased from Sigma-Aldrich (St Louis, MO, USA) and Baker Chemical (Phillipsburgh, NJ, USA), respectively. 4′-Hydroxy-3′-methoxyacetophenone (APO) was purchased from Tokyo Chemical Industry (Tokyo, Japan). Astaxanthin (ATX) was obtained from Sigma-Aldrich (St Louis, MO, USA). Hydroxycaproic acid (HCA) was supplied by Aaron Pharmatech (Shanghai, China). All reagents and chemicals were employed as received without any purification. HCA was used instead of PCL in *in vitro* experiments.

2.2 Fabrication of PCL/MH microspheres containing BA

PCL (1.0 g) and BA (0.5 mg of APO or 3.0 mg of ATX) were dissolved in 10.0 mL of DCM. Magnesium hydroxide solution (100 mg of MH/1.0 mL of distilled water) made of ultra-high nano-disperser was dispersed in a PCL solution. After mixing with the vortex mixer, they (oil phase) were injected to the oil tank of an apparatus of Shirasu porous glass (SPG) membrane emulsification. This apparatus was soaked into 200 mL of 2.0 wt% (w/v) PVA solution (continuous phase), and the SPG membrane was stored in the solution under gentle agitation with a stirrer at room temperature for 1 h. The nitrogen gas that was passed into the tank forced the dispersion droplets using stainless steel module with SPG membrane to a continuous phase containing a dispersion stabilizer. SPG membranes with pore sizes of 30 μm were utilized. The emulsion was poured into 100 mL of 2.0 wt% (w/v) PVA solution after the membrane emulsification. Then solvent evaporation at room temperature was performed at 250 rpm for 12 h. Monodisperse polymer microspheres were separated by centrifugation and rinsed with distilled water three times.

2.3 Characterization of PCL/MH microspheres containing BA

The prepared microspheres were demonstrated by optical microscopy (CKX53, Olympus, Tokyo, Japan) and the size was determined using the Image J software. The surface morphology and magnesium elemental mapping of the microspheres were observed through scanning electron microscopy (SEM; S-4800, HITACHI, Tokyo, Japan). The MH content in PCL microsphere was analyzed using thermogravimetric analysis (TGA, TGA 4000 instrument, PerkinElmer, USA). Roughly, 3 mg of PCL composites was heated at a heating rate (10 °C min^{-1}) from room temperature to 800 °C under nitrogen flow (19.8 mL min^{-1}). The amount of MH content in PCL composites was analyzed from the mass change *versus* the temperature curve.

2.4 *In vitro* degradation and release test

Each specimen of the manufactured microsphere groups was weighed 100 mg and immersed in a glass vial filled with 2 mL of phosphate-buffered saline (PBS, pH 7.4) solution. This

experiment was performed to accelerate the degradation ratio of PCL in PBS solution at 60 °C. The change in the pH of the microspheres was measured using a pH meter (FP20, Mettler-Toledo GmbH, Schwerzenbach, Switzerland) over time. The degraded microspheres were taken out of the solution for a predetermined time. The residual weight was calculated after drying overnight in the drying oven from the following equation.

$$\text{Residual weight } (\%) = 100 - [(\text{initial weight} - \text{final weight})/(\text{initial weight}) \times 100]$$

The amounts of ATX and APO on the microspheres were evaluated using the remaining solutions with a microplate reader (SpectraMax M2, Molecular Devices, San Jose, CA, USA) and by high-performance liquid chromatography (HPLC, Agilent, Santa Clara, CA, USA) with 480 and 275 nm of UV wavelength, respectively.

2.5 Mechanical characterization of the hydrogels

Rheometer (KINEXUS Pro+, Malvern instruments, USA) to measure the fluid properties of conventional hyaluronic acid filler and hyaluronic acid filler with microspheres was used. The measurement conditions were a parallel plate type with a diameter of 20 mm, Gap plate of 2000 μm and 25 °C. Fluidic properties were measured from the response by adding to the sample a static vibration shear deformation of $\gamma = \gamma^0 \sin \omega t$, which gradually increases to the angular frequency = ω (t) over time (t) while maintaining a constant strain amplitude (γ). Each frequency then gradually increased to the algebraic scale to ω = 0.025–10 rad s^{-1}. From this, the storage modulus (G'), viscosity (G''), and complex viscosity (G^*) were measured.

2.6 Cell culture

Human dermal fibroblasts (hDFs; PCS-201-012, ATCC, VA, USA) were grown in Dulbecco's Modified Eagle's Medium (DMEM; Hyclone, UT, USA) containing 1% antibiotic–antimycotic solution (Gibco, Grand Island, NY, USA) and 10% fetal bovine serum (FBS; Hyclone, Logan, UT, USA) at 37 °C in a humidified atmosphere with 5% carbon dioxide (CO_2). The cells were grown in a T75 tissue culture flask until cells reached 90% confluence. The cells were seeded into 96 well culture plates (1×10^4 cells per well). After a day of incubation, the cell viability of the cells treated with 100 mM PCL, PCL/MH, and PCL/MH/BA, respectively, was measured for 6 h using a cell counting kit-8 (CCK-8) assay (Dojindo Molecular Technology, Inc., Japan). Cell viability was evaluated using a live/dead viability/cytotoxicity kit (Invitrogen, Thermo Fisher Scientific., USA) assay. The cells were rinsed using PBS solution and exposed to ethidium homodimer-1 (2 μM) and calcein AM (4 μM) solutions at 37 °C for 30 min. The fluorescence images were obtained using a microscope (U-RFL-T, Olympus, Japan).

2.7 *In vitro* wound healing assay

The hDFs were seeded into 6 well culture plates (2×10^5 cells per well) and allowed to make a confluent monolayer. The monolayer of cells was scratched with a micropipette tip (1 mL) to form an artificial wound. After disruption, the culture plate was gently rinsed twice with fresh PBS solution to remove the detached cell debris and then treated with 100 mM PCL, PCL/MH, and PCL/MH/BA for 6 h, respectively. Wound closure was calculated as a percentage of the wound area and quantitated using the Image J software.

2.8 RNA isolation and real-time quantitative PCR

Total cellular RNA was extracted using AccuPrep® universal RNA extraction it (Bioneer, Korea). The extracted RNA (1 μg) was reverse transcribed to cDNA using a PrimeScript RT reagent kit (Takara Biotechnology, Japan). The quantitative real-time PCR was accomplished using a Power SYBR™ Green PCR Master Mix (Applied Biosystems, CA, USA) with a QuantStudio3 real-time PCR system (Applied Biosystems, Thermo Scientific., MS, USA). All values were calculated with the 18s rRNA and the 2-ΔΔCt method. The followed PCR primer pairs were used: sense 5′-gatgagtacaaaagtcctgatcca-3′ and antisense 5′-ctgcagccactggttctgt-3′ for IL-6; sense 5′-gcaattattccccatgaacg-3′ and antisense 5′-gggacttaatcaacgcaagc-3′ for COX-2; sense 5′-gggattccctggacctaaag-3′ and antisense 5′-ggaacacctcgctctcca-3′ for COL1A1; sense 5′-agtccaggagcaccattagc-3′ and antisense 5′-tggtggtaaaggcgaaatg-3′ for COL3A1; sense 5′-gctaaccttgatgctataactacga-3′ and antisense 5′-tttgtgcgcatgtagaatctg-3′ for MMP1; sense 5′-ccccaaaacggacaaagag-3′ and antisense 5′-cttcagcacaaacaggttgc-3′ for MMP2; sense 5′-ctactgaggagccagcgtcta-3′ and antisense 5′-ctgcccatcatcatgacct-3′ for P16; sense 5′-ccgaagtcagttccttgtgg-3′ and antisense 5′-catgggttctgacggacat-3′ for P21; sense 5′-ccctttttggacttcaggtg-3′ and antisense 5′-aggccttggaactcaaggat-3′ for P53; sense 5′-agtacctgaaccggcacct-3′ and antisense 5′-gccgtacagttccacaaagg-3′ for BCL2; sense 5′-catcatgggctggacattg-3′ and antisense 5′--gggacatcagtcgcttcagt-3′ for BAX; sense 5′-agacctgaaaaatggcttcg-3′ and antisense 5′-cggaaaacctcctctgtgtc-3′ for BAK.

2.9 ROS scavenging activity

For visualization of intracellular ROS, the cells (2.5×10^4 cells per well) were incubated on a 96-well microplate in hydrogen peroxide-containing DMEM/10% FBS with PCL, PCL/MH, or PCL/MH/BA. After 24 h, staining was performed with a cellular ROS assay kit (ab113851, Abcam, MA, USA) following the manufacturer's protocol. Briefly, the cells were incubated with 2′,7′-dichlorofluorescin diacetate (DCFDA) to visualize ROS and stain the nuclei for 45 min at 37 °C in the dark, and then washed twice with PBS solution and imaged by fluorescence microscopy (Olympus IX 71 microscope, Center Valley, PA, USA). ROS production was estimated by fluorescence intensity (excitation/emission = 485/535 nm) and the fluorescence intensity was evaluated using the Image J software.

2.10 Immunofluorescence analysis

The cells were cultured to confluence on 24-well plates and PCL, PCL/MH, or PCL/MH/BA were treated and incubated for 24 h. The cells were washed twice with PBS solution, fixed with 4% PFA solution for 20 min, and then blocked by 1% FBS/0.3% Triton X-100 solution for 30 min. The cells were probed with a collagen type I rabbit antibody (Novus, MO, USA) in 5%

FBS/0.1% Triton X-100 solution at 4 °C overnight. Afterward, the samples were rinsed twice with PBS solution and incubated with Alexa-Fluor 568 goat anti-rabbit secondary antibody (Molecular Probes Inc., OR, USA) in 5% FBS/0.1% Triton X-100 solution at 25 °C for 1 h. After rinsing with PBS solution, the samples were mixed with Vectashield mounting medium/DAPI (Vector, CA, USA). The samples were imaged using a Zeiss LSM880 confocal laser-scanning microscope (Carl Zeiss MicroImaging GmbH, Jena, Germany).

2.11 Western blot analysis

The cells were resuspended in RIPA lysis buffer containing a protease inhibitor. The supernatants were blended with Laemmli buffer for 10 min at 105 °C. The samples were loaded to 10% sodium dodecyl sulfate-polyacrylamide gel electrophoresis (SDS-PAGE) and transferred to a nitrocellulose membrane. After a blocking process with TBST solution containing skimmed milk to reduce the background, the samples were incubated with primary antibodies of IL-6Rα (SC-37308, Santa Cruz Biotechnology, CA, USA), anti-collagen 1 antibody (ab34710, Abcam, MA, USA), and GAPDH (5174T, Cell signaling Technology, MA, USA), and secondary antibody of horseradish peroxidase (HRP)-linked anti-rabbit was used.

2.12 Animals and histological evaluation

All animal procedures were performed in accordance with the Guidelines for Care and Use of Laboratory Animals of CHA University and approved by the Animal Ethics Committee of IACUC210029. Eight-week-old male BALB/c mice, weighing between 14 and 19 g, were used in the study. The mice were under general anesthesia using isoflurane (TerrellTM Isoflurane, Piramal Critical Care Inc., USA). Hair was shaved and the exposed skin was sterilized with ethanol. Then 0.1 mL of the PCL hydrogels was subcutaneously injected into the left and right dorsal regions using 21 G needles. At 4, 8, and 16 weeks post injection, mice were sacrificed and evaluated. The samples were embedded in paraffin and sectioned at 5 μm. The sectioned slides were stained with hematoxylin and eosin (H & E; Abcam, United Kingdom) and Masson's trichrome (MT; VitroVivo Biotech, MD, USA) following the manufacturer's instructions, respectively.

2.13 Statistical analysis

All results were analyzed using the GraphPad Prism software 7 (CA, USA). Differences between groups were evaluated using one-way analysis of variance (ANOVA) with Tukey's multiple comparison post-test and p values below 0.05 were deliberated as statistically significant ($*p < 0.05$; $**p < 0.01$; $***p < 0.001$; $****p < 0.0001$).

3. Results and discussion

3.1 Milling of MH

The fabrication process of PCL/MH microspheres containing BA is illustrated in Fig. 1A. To improve the dispersion stability of MH, an ultra-high nano-disperser was used to control the size of MH particles. As shown in Fig. S1A,† the various sizes of the non-milled MH particles ranged from 0.3 to 100 μm, whereas the milled MH particles were reduced in size to the nano scale (50–600 nm). The non-milled and milled MH particles were dispersed in water at room temperature for 1 h. After 1 h, the non-milled MH particles sank to the bottom of the vial while the milled MH particles were still dispersed in water. In total, the size of the milled MH particles increased to 120–700 nm after the 1 h dispersion. The surface of the MH particle contained many hydroxyl groups, so the dispersibility was high in a polar solvent compared to a non-polar solvent.[35] However, the non-milled MH particles had a size at the micron scale and poor dispersion stability even in water, a polar solvent.[36] Therefore, the dispersion stability increased by reducing the size of the MH particles to the nanoscale using an ultra-high nano-disperser.

3.2 Characterization of PCL/MH microspheres

Microspheres of uniform size were produced using a water-in-oil-in-water (W/O/W) emulsion method with a membrane fluidic device. In addition, the microspheres were manufactured with the addition of MH and various BA. The morphology, magnesium elemental mapping, and size of microspheres with added BA, were determined by SEM. The morphology of microspheres with added MH was rougher and more microporous than PCL microspheres (Fig. 1B). In the magnesium elemental mapping, many dots were observed when MH was added. The size of the microspheres was found to be approximately 30–40 μm in all groups (Fig. 1C) and microspheres of almost uniform size were observed. As PCL, APO, and ATX were dissolved in the oil phase (DCM), it was possible to prepare a basic emulsion, but the hydrophilic MH required the W/O/W double emulsion method to be loaded into the microspheres.[37] In order to safely use polymeric microspheres as skin fillers, the particle size must be uniformly controlled.[38] Too small a particle size could cause capillary embolism. On the other hand, a large particle size is difficult to use as a filler through injection due to the pressure when passing through the syringe needle.[39] We considered all cases, and fabricated all microspheres to a size of 30–40 μm. The surface of the PCL microsphere was observed to be smooth. However, in the group containing MH, the microspheres that formed were roughened.[40] This was presumed to be due to the high hydrophilicity of MH affecting the stability of the secondary emulsion. In the magnesium elemental mapping image, the dots representing Mg^{2+} are evenly stamped on the surface of the microspheres including MH. This demonstrates that MH is uniformly distributed in the microspheres. In a previous study, excellent anti-inflammatory effect was observed for an MH content of 10% or more compared to the polymer.[36,41] We adjusted the feed amount to approximately 15%, assuming MH is lost during the sealing process. In all MH groups, the encapsulation efficiency was over 94%, and represented over 13% of the total mass of the microspheres.

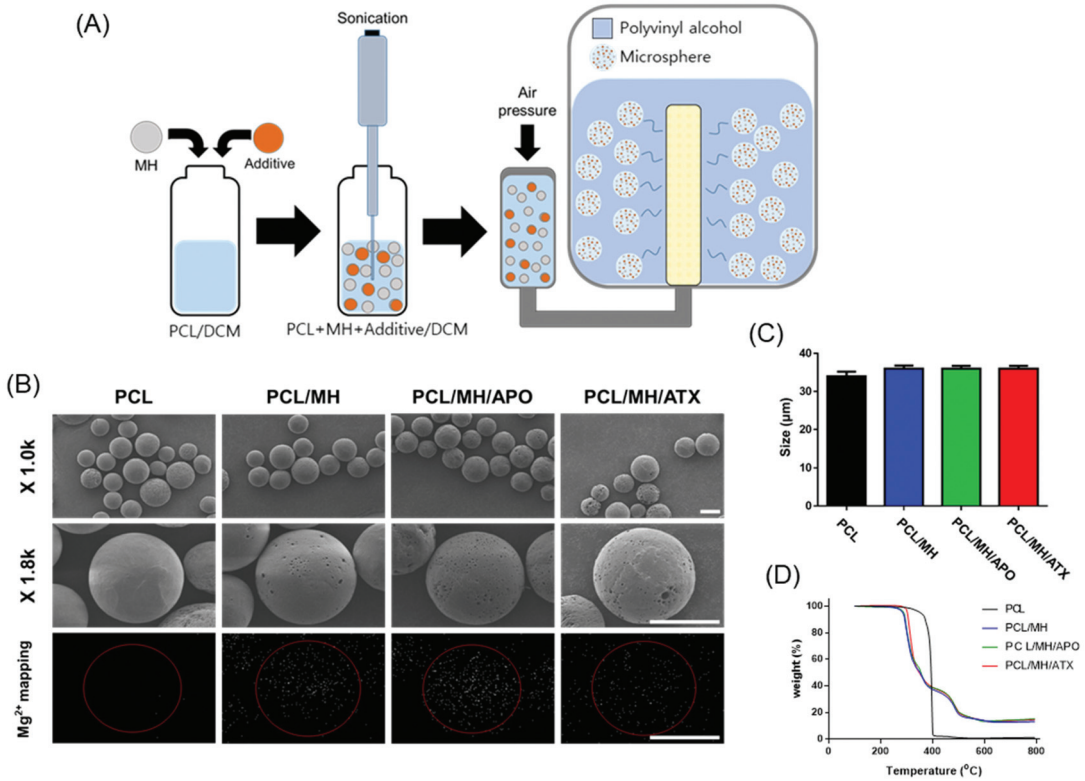

Fig. 1 (A) Schematic illustration of polymer microsphere preparation containing magnesium hydroxide nanoparticles. (B) SEM and EDS images for magnesium elemental mapping images of microspheres (scale bar: 50 μm). (C) Size of microsphere. (D) TGA thermograms of microspheres.

3.3 Quantification of MH contained in the microspheres

TGA was conducted to evaluate the loading content and efficiency of MH in the microspheres. In Fig. 1D, the comparisons of thermograms of PCL/MH microspheres containing PCL/MH and BA are indicated. For all groups, the weight greatly decreased as PCL was degraded between 300 and 400 °C. After 500 °C, only the residual weight of the inorganic MH ceramic remained. As listed in Table 1, when 15% weight of MH was added to PCL, the MH groups were loaded with 13.1, 13.3, and 13.5% in the PCL/MH, PCL/MH/APO, and PCL/MH/ATX microspheres, respectively. The encapsulation efficiency was shown to be 94.5, 96.0, and 97.4%, respectively.

3.4 *In vitro* degradation behavior of the microspheres

HCA produced by PCL hydrolysis could cause the surrounding environment to assume acidic conditions, leading to an inflammatory response. To confirm the neutralization effect of MH, changes in pH and weight over time were determined for microspheres from all groups in a PBS solution at 60 °C. Since PCL has a very slow degradation rate of about two years, these experiments were conducted under severe conditions at high temperature. PCL microspheres gradually acidified the solution to a pH of 6.68 by the 28th day (Fig. 2A). All groups with added MH were neutralized by the 5th day in the PBS solution, which was acidified as PCL degraded, and maintained a pH of 8 until the 28th day. Fig. 2B shows the percentage of initial weight remaining during decomposition over time. The results from all groups showed similar weight loss until the 5th day. The remaining weight on the 28th day was 82.32, 85.19, and 84.23% for PCL/MH, PCL/MH/APO, and PCL/MH/ATX microspheres, respectively, and the PCL group was the most degraded. PCL is degraded and excreted as HCA through metabolic processes in the body. HCA is known to have low toxicity

Table 1 Quantity of MH and BA contained in the microspheres

	Magnesium hydroxide (MH)			Bioactive agent (BA)	
Factor	PCL/MH	PCL/MH/APO	PCL/MH/ATX	APO	ATX
Feeding amount (mg)	800	800	800	0.5	3
Loading amount (mg)	755.6	768	779.2	0.42	2.64
Encapsulation efficiency (%)	94.5 (±2.7)	96 (±1.0)	97.4 (±4.8)	88.2 (±1.5)	88.2 (±3.2)
Mg (%)	13.1	13.3	13.5	—	—

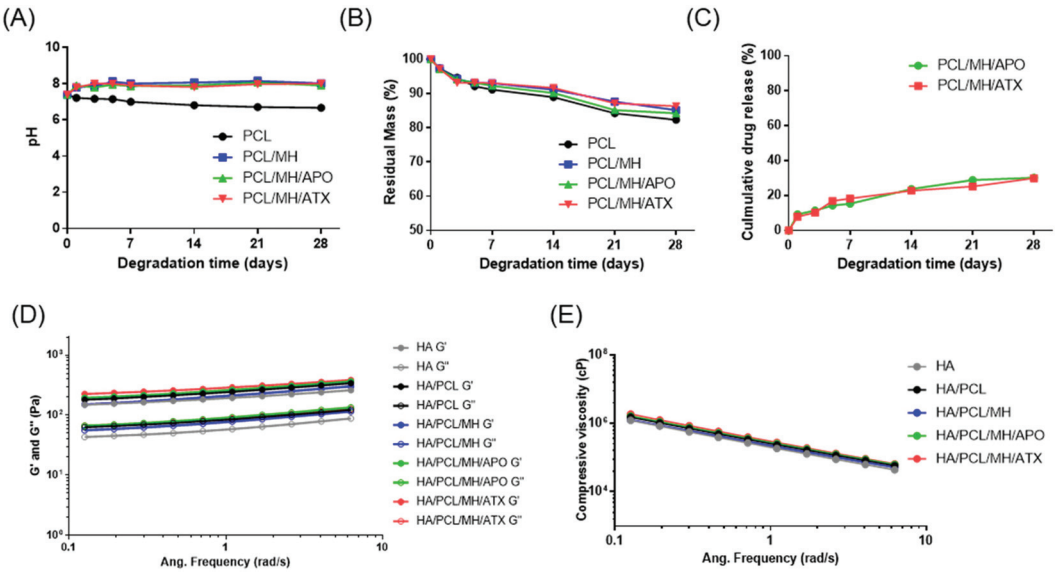

Fig. 2 (A) *In vitro* degradation behavior of microspheres: change of (A) pH and (B) residual weight. (C) Bioactive agent (BA) release profile in PBS solution at 60 °C. Mechanical properties of the hydrogel filler with microspheres, in terms of (D) elasticity (G'), viscosity (G''). (E) Complex viscosity.

but is an acidic monomer in nature.[6] As PCL is degraded, and HCA accumulates in the surrounding tissues, these tissues change to an acidic environment. An acidic environment could cause side effects of inflammation or necrosis in surrounding tissues. In addition, the acidic environment could accelerate the hydrolysis of the polymer, which may impair its decomposition stability. In the groups containing MH, the microspheres were degraded, and internal MH was released to neutralize PCL, thereby maintaining a pH of 8. In addition, the weight decreased the most in the PCL group, demonstrating that MH increased the degradation stability of the microspheres.

3.5 BA encapsulation efficiency and release behavior

The BA, such as APO (0.5 mg) and ATX (3 mg), was added to 1.25 g of PCL/MH. HPLC was used to determine a loading content of 0.42 mg of APO in 1.25 g of PCL/MH microspheres, whereas the loading content of ATX was confirmed to be 2.64 mg by UV-spectrometry. The release behavior of the BA was monitored for 28 days in a PBS solution at 60 °C. On the first day, APO and ATX were released at a rate of 9.16% and 7.82%, respectively. By the 28th day, the BA was slowly released at 30.12% and 29.87% of the total loading, due to the slow degradation rate of PCL (Fig. 2C). When APO and ATX were added to the PCL/MH microspheres, the encapsulation efficiency was 83.18 and 88.15%, respectively. It appeared that the hydrophobic APO and ATX were not lost due to exposure to water during the manufacturing and washing process, similar to MH. Likewise, the BA loaded onto the PCL microspheres also demonstrated a slow-release behavior.

3.6 Mechanical properties of a hydrogel filler using microspheres

The effect of the addition of microspheres on the elasticity (G'), viscosity (G''), and complex viscosity of the cross-linked HA gel is shown in Fig. 2D, E, and Table S1.† The addition of microspheres in the cross-linked HA gel tended to increase the measured values of G', G'', and complex viscosity in all measured frequencies (0.01–1.0 Hz). For example, the complex viscosity for the addition of the PCL, PCL/MH, PCL/MH/APO, and PCL/MH/ATX microspheres was measured at 1.0 Hz as 1 533 900, 1 287 600, 1 639 200, and 188 600 mPa, respectively (Table S1†). The elasticity, viscosity, and complex viscosity are important physical properties.[42] Here, the increased elasticity, viscosity, and complex viscosity by the addition of the microspheres demonstrated that they could be sufficiently used as cross-linked hyaluronic acid injections.[43] In addition, it was found that the physical properties of the HA-based hydrogel were not significantly different with or without BA on the surface of the microspheres.

3.7 *In vitro* cell proliferation of dermal fibroblasts

Human fibroblast cells were used to verify the neutralizing effect of MH on the degradation products of PCL. The toxicity of the PCL/MH, in relation to the MH content, was determined under various PCL concentration conditions. Here, the cell viability decreased as the PCL concentration increased. In contrast, the cell viability improved as the concentration of added MH increased (Fig. S2†). When 100 mM of PCL was used in the treatment, the cell survival rate was 73.51%. This was assumed to be the minimum concentration required to damage cells, and the following experiments were set to a PCL concentration of 100 mM. The live/dead staining images displayed more live cells in the PCL/MH, PCL/MH/APO, and PCL/MH/ATX groups compared to the PCL group, revealing improved cell compatibility (Fig. 3A and B). Therefore, the addition of MH and BA saw the improvement of cell growth conditions compared to the cells damaged by PCL alone. The cell viability lowered to

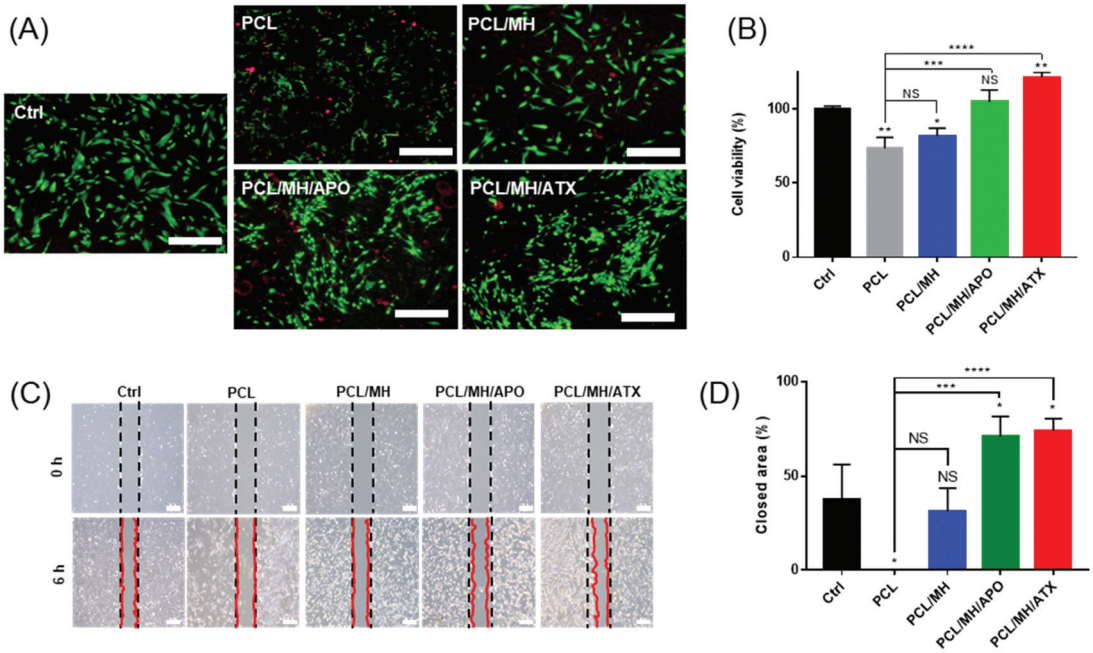

Fig. 3 *In vitro* cell proliferation of dermal fibroblasts: (A) representative live/dead assay images (scale bar: 500 μm) and (B) quantitative analysis of cell viability. (C) Wound healing effect using optical microscopic images (scale bar: 200 μm). (D) Quantitative analysis of the closed wounded area at six hours after incubation.

73.51% in the presence of just PCL, and significantly increased to 81.70, 104.89, and 121.59% with the addition of MH, MH/APO, and MH/ATX, respectively. Because of the MH nanoparticles, the PCL/MH, PCL/MH/APO, and PCL/MH/ATX groups resisted pH changes induced by the PCL degradation byproducts. Furthermore, the supplementation of BA stimulated the proliferation of human fibroblast cells.

3.8 *In vitro* wound healing effect on dermal fibroblasts

The effect of wound healing by MH on the PCL in human fibroblast cells was investigated. The cells were cultured and

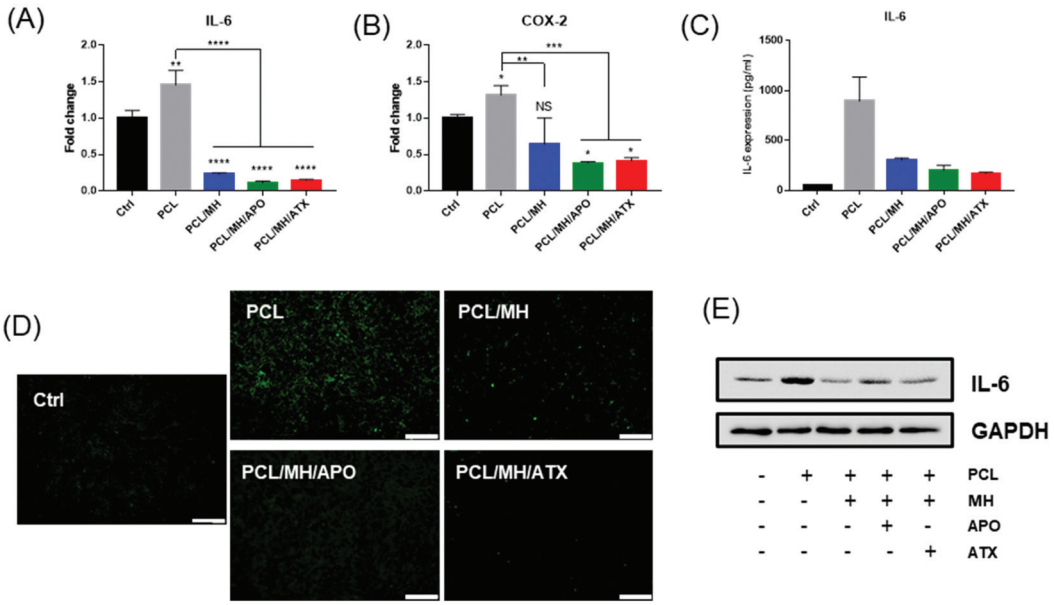

Fig. 4 Anti-inflammatory effect on dermal fibroblasts: qPCR data for inflammatory (A) IL-6 and (B) COX-2. (C) Quantitative ELISA for IL-6 expression. (D) ICC staining images of IL-6 containing cells (scale bar: 500 μm). (E) Western blot analysis for the expression of IL-6.

then scratched with a tip to simulate wound damage. PCL, PCL/MH, and PCL/MH/BA were then added to the cells, and the wound sites were observed after 6 h (Fig. 3C). The damaged sites of all MH-added groups were significantly reduced compared to those of the PCL group. Here, the PCL inhibited cell proliferation and migration by inducing inflammation of the cells with the acidic PCL degradation products. As the acidification by PCL was successfully neutralized by the MH, the proliferation and migration of inhibited cells were successfully enhanced. After 6 h, the open area of the plate was significantly reduced. The MH-treated group exhibited a significant reduction in the damaged area compared to the PCL-treated group. The acidic environment leads to reactive oxygen species in the fibroblast cells, which has a negative effect on cell proliferation, and causes cell death.[44,45] Notably, the wound opening significantly decreased in the PCL/MH/APO and PCL/MH/ATX groups, making them effective in wound healing and tissue regeneration. In Fig. 3D, the closed area of the PCL/MH/APO (70.9%) and the PCL/MH/ATX (74.1%) was significantly greater than due to the PCL/MH (31.4%). The culmination of these results suggest that BA performs effectively in wound healing.

3.9 *In vitro* anti-inflammatory effect

To demonstrate the anti-inflammatory response of MH and BA on dermal fibroblast cells in acidic environments, IL-6 and COX-2 expression levels were determined by gene representations (Fig. 4). The initial IL-6 and COX-2 expression levels were similar among groups treated with PCL, HCA/MH, and BA but only groups treated with PCL had significantly increased IL-6 and COX-2 expression after 6 h. The PCL group showed approximately seven and three times the gene expression of IL-6 and COX-2, respectively, compared to the control group. Additionally, the MH-treated groups were observed to have a similar degree of gene expression (IL-4: PCL/MH 0.22, PCL/MH/APO 0.12, and PCL/MH/ATX 0.14; COX-2: PCL/MH 0.62, PCL/MH/APO 0.39, and PCL/MH/ATX 0.42). These results implied that MH successfully decreases inflammatory reactions caused by PCL. Riemann *et al.* reported a relationship between the acidic environment and fibrosis and inflammation.[1,46] They determined that an acidic environment leads to pathological genes in fibroblasts and produces an inflammatory response that can cause tissue remodeling. Meanwhile, in the PCL/MH-treated groups con-

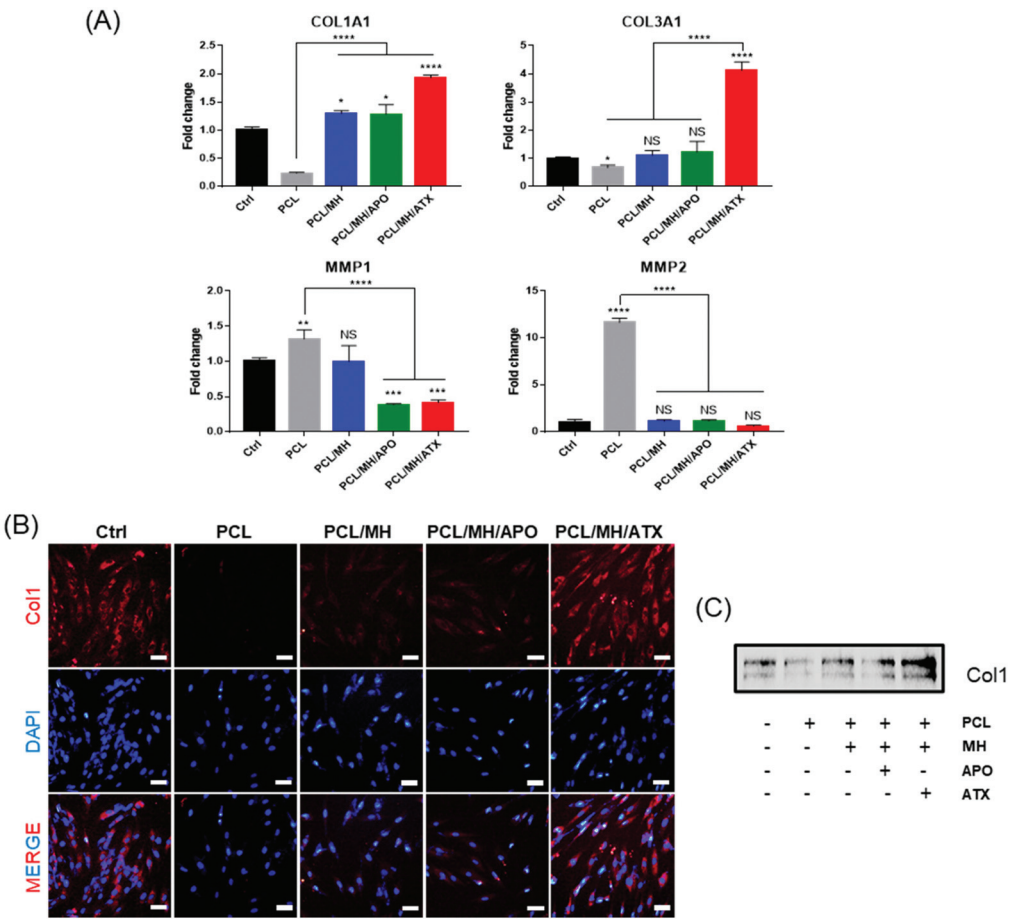

Fig. 5 Collagen production recovery of dermal fibroblasts: (A) qPCR data for collagen synthesis (COL1A1 and COL3A1) and degradation factors (MMP1 and MMP2) in dermal fibroblasts. (B) Representative confocal COL1 immunofluorescence images (scale bar: 50 μm). (C) Western blot analysis presenting the expression of COL1.

taining BA, the expression levels of IL-6 and COX-2 were not significantly different from that in the control group, regardless of time elapsed. The protein expression level and fluorescence image for IL-6 was akin to that of the gene expression level (Fig. 4D and E). The protein expression and fluorescence intensity of IL-6 were remarkably altered in the PCL-treated group but not in the PCL/MH-treated group. These results suggest that neutralization of degradation products by MH can inhibit the inflammatory reaction.

3.10 *In vitro* recovery of collagen production

Collagen production is important to restore wrinkled skin after filler injection. To verify collagen production in dermal fibroblast cells by acidic decomposition products, we investigated the expression of genes related to collagen production (COL1A1 and COL3A1), and decomposition (MMP1 and MMP2) (Fig. 5A). When treated with PCL, the expression of COL1A1 and COL3A1 was higher than that of the control group after 6 h. In particular, the gene expression of PCL/MH/ATX was significantly increased compared to other groups. The gene expression levels of the collagen decomposition factors, MMP1 and MMP2, increased when treated with PCL compared to the control group. However, MH-treated groups containing APO and ATX were significantly decreased. For confocal microscopy, the cells were treated with PCL, PCL/MH, or PCL/MH/BA, and the expressed collagen was stained with COL1 antibody (Fig. 5B). Collagen expression significantly decreased in the PCL-treated cells compared to that in the control group, but collagen expression was maintained in the PCL/MH-treated groups containing BA. Notably, the collagen expression level was the highest for the PCL/MH/ATX group. These results coincided with similar data from western blot experiments (Fig. 5C). This suggests that the addition of MH and BA prevents collagen reduction and thus improves the total amount of collagen.

3.11 *In vitro* anti-senescent effect

To confirm the effect of MH and BA on skin aging, the gene expression of biological indicators of cell aging (P16, P21, and P53) were investigated (Fig. 6A). After 6 h, gene expression of P16, P21, and P53 in the PCL-treated group increased remarkably. The groups with MH and BA showed a lower expression in the senescent biomarkers than the PCL group, demonstrating suppression of the gene expression raised by PCL. This implies that MH and BA suppress cell aging caused by PCL. Moreover, the gene expression of P16, P21, and P53 decreased when treated with MH. From these results, MH can also inhibit senescence induced by acid stress. Hyper-proliferation signals cause increased levels of p16, resulting in cell death or cell cycle arrest through the pRb pathways.[47] For many cell types, especially in humans, p16 contributes to the cell cycle arrest that appears after hyper-proliferation stress. p21 is a cell cycle inhibitor while p53 is a tumor suppressor. When cells are damaged, p21 and p53 work together to inactivate the cyclin–Cdk complex, which intercedes G1 and G2/M arrest.[48] Therefore, PCL/MH/BA affected the senescence of hDFs by decreasing mRNA expression of the p16, p21, and p53 senes-

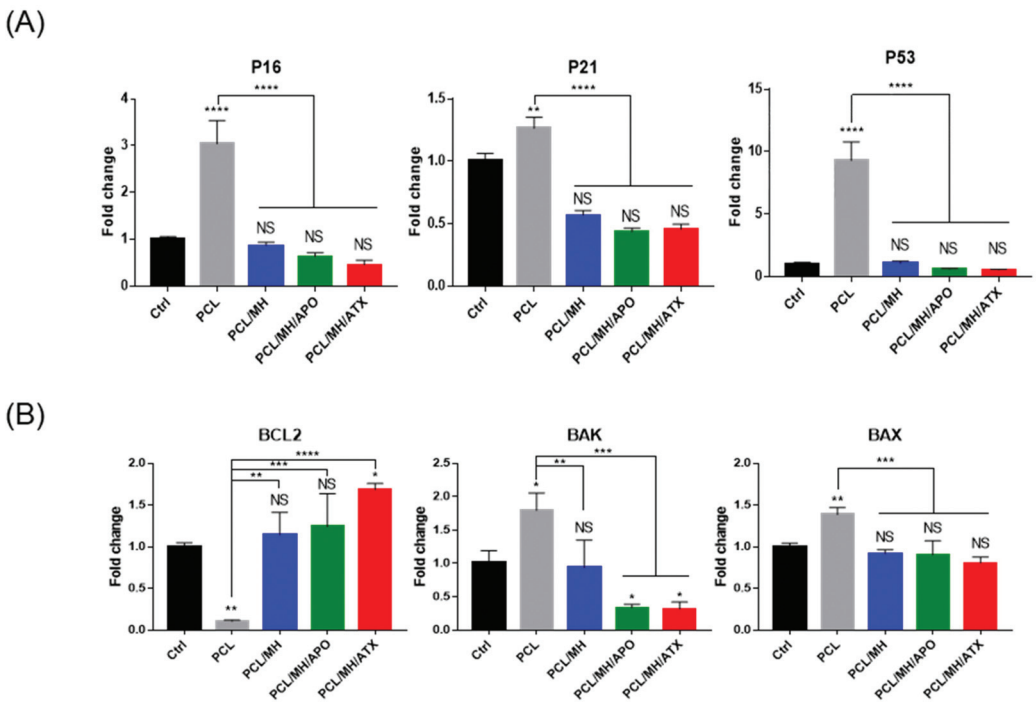

Fig. 6 Anti-senescent and anti-apoptotic effects of dermal fibroblasts: qPCR data of (A) anti-senescence (P16, P21, and P53) and (B) anti-apoptosis (BCL2, BAK, and BAX) genes.

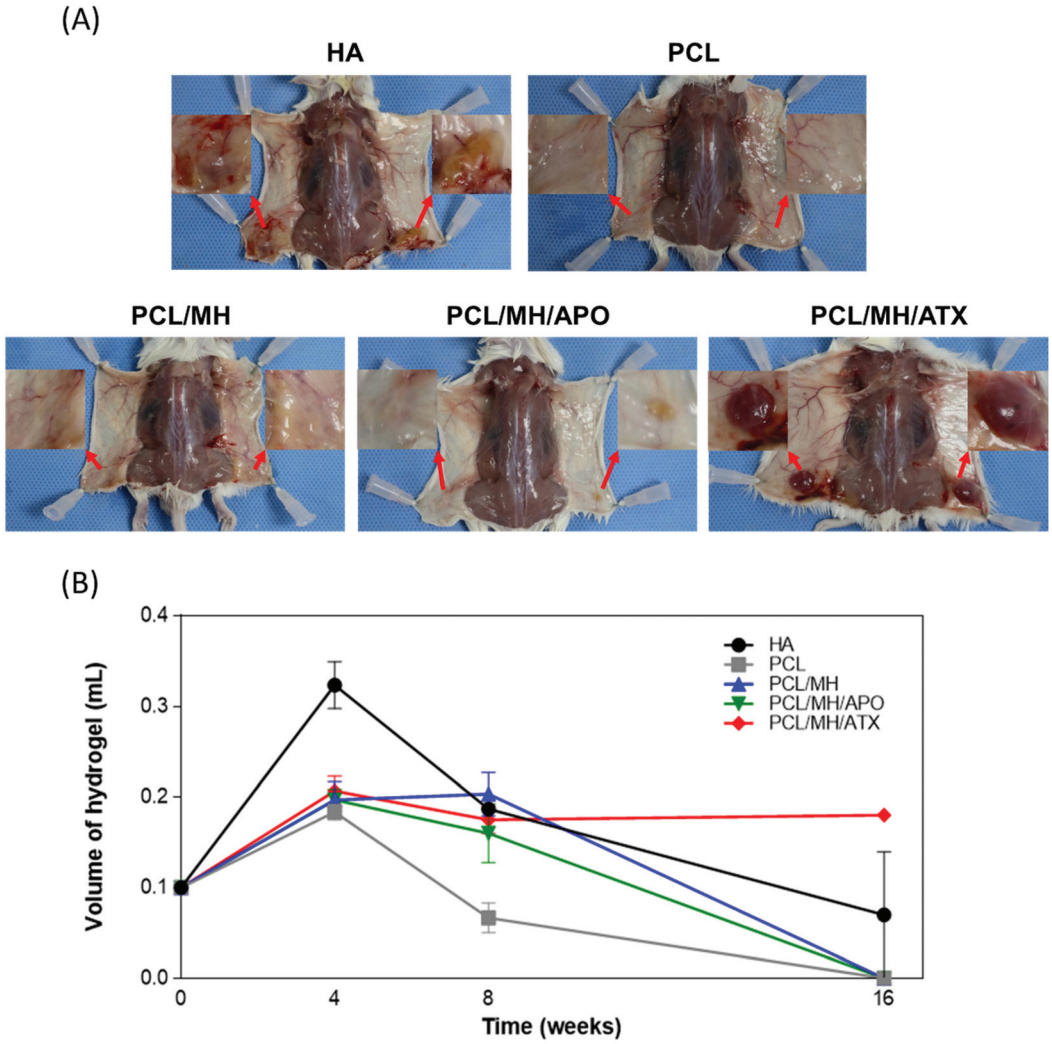

Fig. 7 *In vivo* changes in PCL hydrogel volumes after 16 weeks: (A) images of the PCL hydrogel volumes at 16 weeks, and (B) quantitative analysis of the PCL hydrogel volumes over 16 weeks.

cence biomarkers. These results suggest that the PCL/MH/BA could potentially be used as an anti-aging filler.

3.12 *In vitro* anti-apoptotic effect

To investigate the effect on apoptosis by the PCL/MH/BA, we examined the gene expression of three cellular apoptosis biomarkers: BCL2, BAK, and BAX (Fig. 6B). After 6 h, BCL2 gene expression noticeably decreased in the PCL-treated group, and increased in the PCL/MH- and PCL/MH/BA-treated groups. On the other hand, BAK and BAX gene expression increased in the PCL-treated group compared to the control group, and decreased in the PCL/MH- and PCL/MH/BA-treated groups. BAK expression in the PCL/MH-treated group was similar to the control group while in PCL/MH/BA it was much lower than in PCL/MH. Cell apoptosis is highly connected with cell proliferation and plays a crucial role in human development.[49] The BCL2 factor plays an indispensable role in the mitochondrial apoptosis pathway. Both BAK and BAX expression are important inducers of mitochondrial apoptosis in response to several stimuli surrounding DNA damage.[50,51] In summary, the PCL/MH/BA effectively increased BCL2 expression levels and suppressed BAK and BAX expression levels, indicating that the PCL/MH/BA is an efficient material for dermal fillers.

3.13 *In vivo* durability of the functional PCL polymer filler

A dermal filler aims to void space and increase tissue volume. We evaluated the volume durability of the functional PCL fillers *in vivo* at 4, 8, and 16 weeks after subcutaneous injection in mice. As shown in Fig. 7A and B, the injected filler was barely observed in the HA group due to absorption by the body. A thin film-like residual substance was observed for the PCL/MH and PCL/MH/APO groups. However, for the PCL/MH/ATX group, the residue was shown as a clear and perfectly spherical surface. At 4 weeks post-injection, the volume remaining in the HA group increased by 320% due to massive initial gel swelling compared to the PCL (183.3%), PCL/MH

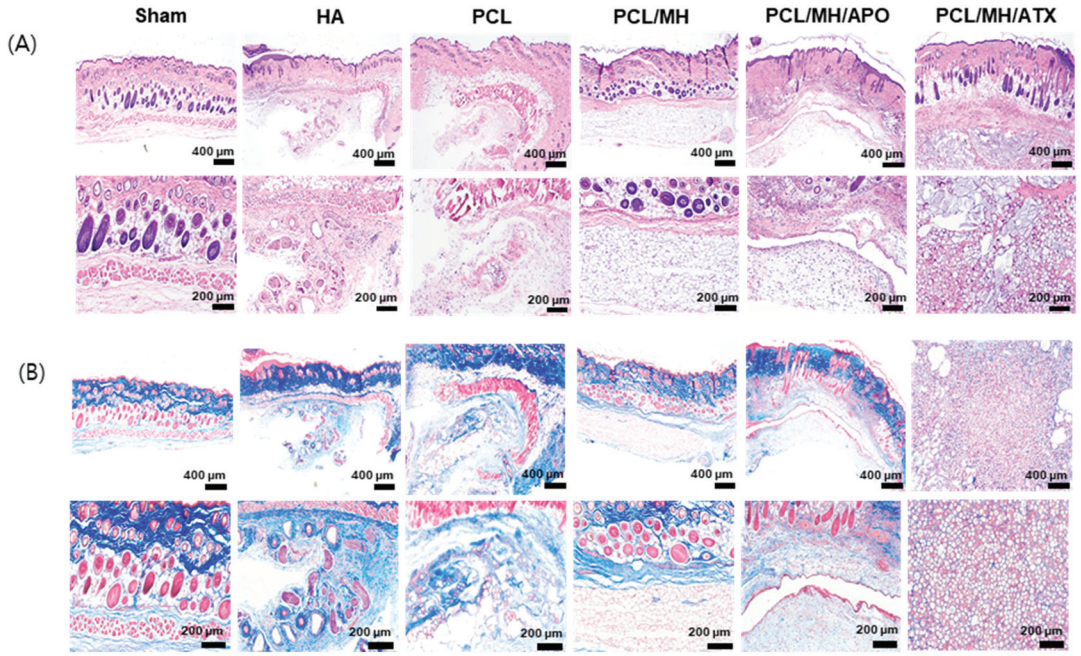

Fig. 8 *In vivo* evaluation of the PCL filler function: (A) H&E and (B) MT staining in a mouse model at 16 weeks post-implantation.

(196.7%), PCL/MH/APO (196.7%), and PCL/MH/ATX (206.7%) groups. At the next time point (8 weeks after injection), the residual volume of the PCL group dramatically decreased. At 16 weeks, among all of the injected groups, PCL/MH/ATX showed the most outstanding volumetric retention effect. In addition, histological analysis was evaluated to verify the internal tissue augmentation. Based on H&E and MT staining images at 4 and 8 weeks, residual HA gel was observed in the HA group. In groups containing microspheres, there were many pores inside the grafted gel that indicated traces of microspheres (Fig. S3 and S4†). In Fig. 8, the residual grafted substances of the HA, PCL, PCL/MH, and PCL/MH/APO treatment hardly remained after 16 weeks. However, traces of microspheres and HA gel were still observed for the PCL/MH/ATX group. Consequently, based on these images, residual mass, and histological investigations, the addition of the PCL/MH/ATX microspheres in the HA hydrogel would be appropriate for a functionalized, long-lasting dermal filler.

4. Conclusions

A functional PCL polymer filler was established to surmount the disadvantages of ordinary polymeric fillers for skincare applications. MH, a biocompatible ceramic, was used to neutralize the degradation byproducts of PCL microspheres after injection into the skin. The BA-added PCL/MH microspheres were uniformly fabricated using a membrane emulsification system. Unlike PCL degradation that has an acidic property, the addition of the PCL/MH/BA microspheres, particularly the PCL/MH/ATX, in HA hydrogel presented promising results for sustained release. In addition, for *in vitro* and *in vivo* tests, PCL/MH/ATX group had the highest enhanced wound healing, anti-inflammation, collagen production, anti-senescence, and anti-apoptotic properties than the other groups. In conclusion, it is expected that the ATX added PCL/MH microspheres could have excellent potential as a multifunctional dermal filler for facial plastic surgery and skincare applications.

Author contributions

The manuscript was written through contributions of all the authors. All the authors have given their approval to the final version of the manuscript.

Conflicts of interest

The authors declare no competing financial interests.

Acknowledgements

This work was supported by Basic Science Research Program (2020R1A2B5B03002344 and 2021R1I1A1A01045745) and Bio & Medical Technology Development Program (2018M3A9E2024579) through the National Research Foundation (NRF) of Korea funded by the Ministry of Education, and the Korea Medical Device Development Fund grant funded by the Korean government (the Ministry of Science and ICT, the Ministry of Trade, Industry and Energy, the Ministry of Health & Welfare, the Ministry of Food and Drug Safety) (202011A05-05), Republic of Korea.

References

1 A. Riemann, A. Ihling, J. Thomas, B. Schneider, O. Thews and M. Gekle, *Biochim. Biophys. Acta, Mol. Cell Res.*, 2015, **1853**, 299–307.
2 J. A. Kim and D. Van Abel, *J. Cosmet. Laser Ther.*, 2015, **17**, 99–101.
3 G. Kogan, L. Šoltés, R. Stern and P. Gemeiner, *Biotechnol. Lett.*, 2007, **29**, 17–25.
4 C. H. Kum, Y. Cho, S. H. Seo, Y. K. Joung, D. J. Ahn and D. K. Han, *Small*, 2014, **10**, 3783–3794.
5 M. A. Woodruff and D. W. Hutmacher, *Prog. Polym. Sci.*, 2010, **35**, 1217–1256.
6 B. Bae, G. Lee, O. Sewoong and K. Hong, *Dermatol. Surg.*, 2016, **42**, 1256–1260.
7 F. de Melo, P. Nicolau, L. Piovano, S.-L. Lin, T. Baptista-Fernandes, M. I. King, A. Camporese, K. Hong, M. M. Khattar and M.-O. Christen, *Clin., Cosmet. Invest. Dermatol.*, 2017, **10**, 431–440.
8 T. R. Kwon, S. W. Han, I. K. Yeo, J. H. Kim, J. M. Kim, J. Y. Hong, B. C. Lee, S. E. Lee, H. S. Moon and H. J. Kwon, *J. Cosmet. Dermatol.*, 2019, **18**, 1002–1008.
9 P. Bastian, R. Bartkowski, H. Köhler and T. Kissel, *Eur. J. Pharm. Biopharm.*, 1998, **46**, 243–254.
10 S. J. Falcone and R. A. Berg, *J. Biomed. Mater. Res., Part A*, 2008, **87**, 264–271.
11 H. W. Lee, S. H. Seo, C. H. Kum, B. J. Park, Y. K. Joung, T. I. Son and D. K. Han, *Macromol. Res.*, 2014, **22**, 210–218.
12 S. W. Choi, Y. Zhang and Y. Xia, *Adv. Funct. Mater.*, 2009, **19**, 2943–2949.
13 J.-S. Choi, S. H. Oh, Y.-M. Kim and J.-Y. Lim, *Tissue Eng. Regener. Med.*, 2020, **17**, 651–658.
14 J. H. Kim, K.-M. Lee, S. H. Han, E. A. Ko, D. S. Yoon, I. K. Park, H.-C. Shin, K. H. Park and J. W. Lee, *J. Tissue Eng.*, 2021, **3**, 2041731421999750.
15 F. de Melo and J. Marijnissen-Hofsté, *Dermatol. Ther.*, 2012, **2**, 1–10.
16 E. Lih, K. W. Park, S. Y. Chun, H. Kim, T. G. Kwon, Y. K. Joung and D. K. Han, *ACS Appl. Mater. Interfaces*, 2016, **8**, 21145–21154.
17 N. Fatima, U. Y. Qazi, A. Mansha, I. A. Bhatti, R. Javaid, Q. Abbas, N. Nadeem, Z. A. Rehan, S. Noreen and M. Zahid, *J. Ind. Eng. Chem.*, 2021, **100**, 40–58.
18 A. Fallacara, S. Manfredini, E. Durini and S. Vertuani, *Facial Plast. Surg.*, 2017, **33**, 87–96.
19 S.-K. Moon, I. W. Cheong and S.-W. Choi, *Colloids Surf., A*, 2014, **454**, 84–88.
20 M.-H. Kim, J.-H. Park, D.-T. Nguyen, S. Y. Kim, D. I. Jeong, H.-J. Cho and D.-D. Kim, *Pharmaceutics*, 2021, **13**, 170.
21 K. Flegeau, O. Gauthier, G. Rethore, F. Autrusseau, A. Schaefer, J. Lesoeur, J. Veziers, A. Brésin, H. Gautier and P. Weiss, *Biomater. Sci.*, 2021, **9**, 5640–5651.
22 W. Park, D. Kim, H. C. Kang, Y. H. Bae and K. Na, *Biomaterials*, 2012, **33**, 8848–8857.
23 A. A. Shamsuri and K. Abdan, *Polymers*, 2021, **13**, 2597.
24 L. Zhang, W. Chai, W. Li, K. Semple, N. Yin, W. Zhang and C. Dai, *ACS Omega*, 2021, **6**, 26990–27006.
25 M. A. Munawar and D. W. Schubert, *ACS Appl. Polym. Mater.*, 2021, **3**, 2889–2901.
26 W. Park, A. C. Gordon, S. Cho, X. Huang, K. R. Harris, A. C. Larson and D.-H. Kim, *ACS Appl. Mater. Interfaces*, 2017, **9**, 13819–13824.
27 E. Lih, C. H. Kum, W. Park, S. Y. Chun, Y. Cho, Y. K. Joung, K.-S. Park, Y. J. Hong, D. J. Ahn and B.-S. Kim, *ACS Nano*, 2018, **12**, 6917–6925.
28 E. Y. Kang, B. Choi, W. Park, I. H. Kim and D. K. Han, *Colloids Surf., B*, 2019, **179**, 161–169.
29 E. Lih, W. Park, K. W. Park, S. Y. Chun, H. Kim, Y. K. Joung, T. G. Kwon, J. A. Hubbell and D. K. Han, *ACS Cent. Sci.*, 2019, **5**, 458–467.
30 K.-S. Park, B.-J. Kim, E. Lih, W. Park, S.-H. Lee, Y. K. Joung and D. K. Han, *Acta Biomater.*, 2018, **73**, 204–216.
31 J.-K. Kim, E.-J. Go, K.-W. Ko, H.-J. Oh, J. Han, D. K. Han and W. Park, *Tissue Eng. Regener. Med.*, 2021, **18**, 613–622.
32 S. R. Savla, A. P. Laddha and Y. A. Kulkarni, *Drug Metab. Rev.*, 2021, **53**, 542–562.
33 E.-M. Noh, J. Park, H.-R. Song, J.-M. Kim, M. Lee, H.-K. Song, O.-Y. Hong, P. H. Whang, M.-K. Han and K.-B. Kwon, *Oxid. Med. Cell. Longevity*, 2016, **2016**, 1–9.
34 D. W. Killilea and B. N. Ames, *Proc. Natl. Acad. Sci. U. S. A.*, 2008, **105**, 5768–5773.
35 R. J. Rohrich, A. Ghavami and M. A. Crosby, *Plast. Reconstr. Surg.*, 2007, **120**, 41S–54S.
36 T. M. Bedair, Y. Heo, J. Ryu, H. M. Bedair, W. Park and D. K. Han, *Biomater. Sci.*, 2021, **9**, 1903–1923.
37 J. A. Burdick and G. D. Prestwich, *Adv. Mater.*, 2011, **23**, H41–H56.
38 T. Segura, B. C. Anderson, P. H. Chung, R. E. Webber, K. R. Shull and L. D. Shea, *Biomaterials*, 2005, **26**, 359–371.
39 H. Sun, Q.-F. Zhang and J.-L. Wu, *Nanotechnology*, 2006, **17**, 2271–2274.
40 S. W. Choi, I. W. Cheong, J. H. Kim and Y. Xia, *Small*, 2009, **5**, 454–459.
41 H. I. Lee, Y. Heo, S.-W. Baek, D.-S. Kim, D. H. Song and D. K. Han, *Polymers*, 2021, **13**, 1979.
42 D. Stocks, H. Sundaram, J. Michaels, M. J. Durrani, M. S. Wortzman and D. B. Nelson, *J. Drugs Dermatol.*, 2011, **10**, 974–980.
43 F. S. Brandt and A. Cazzaniga, *Clin. Interventions Aging*, 2008, **3**, 153–159.
44 A. Riemann, B. Schneider, A. Ihling, M. Nowak, C. Sauvant, O. Thews and M. Gekle, *PLoS One*, 2011, **6**, e22445.
45 M. Parekh, V. Romano, K. Hassanin, V. Testa, R. Wongvisavavit, S. Ferrari, A. Haneef, C. Willoughby, D. Ponzin and V. Jhanji, *J. Tissue Eng.*, 2021, **12**, 2041731421990536.
46 T. M. Bedair, C. K. Lee, D.-S. Kim, S.-W. Baek, H. M. Bedair, H. P. Joshi, U. Y. Choi, K.-H. Park, W. Park, I. Han and D. K. Han, *J. Tissue Eng.*, 2020, **11**, 2041731420967591.
47 E.-Y. Min, I.-H. Kim, J. Lee, E.-Y. Kim, Y.-H. Choi and T.-J. Nam, *Int. J. Oncol.*, 2014, **45**, 47–56.

48 M. Sharifi-Rad, R. Pezzani, M. Redaelli, M. Zorzan, M. Imran, A. A. Khalil, B. Salehi, F. Sharopov, W. C. Cho and J. Sharifi-Rad, *Molecules*, 2020, **25**, 467.
49 S. Nagata, *Annu. Rev. Immunol.*, 2018, **36**, 489–517.
50 P. E. Czabotar, G. Lessene, A. Strasser and J. M. Adams, *Nat. Rev. Mol. Cell Biol.*, 2014, **15**, 49–63.
51 R. J. Youle and A. Strasser, *Nat. Rev. Mol. Cell Biol.*, 2008, **9**, 47–59.